

Polarisation and Brightness Temperature Observations of Venus with the GMRT

Nithin Mohan,¹ Suresh Raju C,^{1*} Govind Swarup² and Divya Oberoi²

¹*Space Physics Laboratory, Vikram Sarabhai Space Centre, ISRO, Thiruvananthapuram 695 022, India*

²*National Centre for Radio Astrophysics, TIFR, Pune University Campus, Post Bag 3, Pune 411 007, India*

Accepted XXX. Received YYY; in original form ZZZ

ABSTRACT

Venus was observed at frequencies of 1297.67 MHz (23 cm), 607.67 MHz (49 cm) and 233.67 MHz (1.28 m) with the Giant Metrewave Radio Telescope (GMRT) during the period of 25th July and 6th September 2015 when it was close to its inferior conjunction. Values of the brightness temperature (T_b) of Venus from these observations were derived as 622 ± 43 K, 554 ± 38 K for 1297.67 and 607.67 MHz frequencies, respectively, are in agreement with the previous observations. The attempt to derive the T_b at 233.67 MHz affirms an upper limit of 321 K which is significantly lower than the previously reported upper limit of 426 K at the same frequency. We also present the dielectric constant (ϵ) values of the Venus surface estimated using the degree of polarisation maps of Venus, derived from the GMRT polarisation observations and theoretical calculations. The ϵ of the Venus surface was estimated to be ~ 4.5 at both the 607.67 MHz and 1297.67 MHz, close to the reported values of ϵ of 4 to 4.5 from the radar-based observations including the Magellan observations at 2.38 GHz (12.6 cm).

Key words: planets and satellites: individual: Venus, terrestrial planets, surface-polarization-techniques: interferometric

1 INTRODUCTION

Observations of the planetary bodies at microwave and radio wavelengths (millimetre (mm), centimetre (cm) and decimetre (dcm)) have made significant contributions towards understanding the planetary atmospheres and their surfaces (DePater 1990, 1991). The albedo of the planetary surface determines the fraction of the solar radiation reflected from the surface and the rest is conducted into the subsurface as heat. Depending upon the surface properties (dielectric constant and surface roughness) and the local thermal equilibrium, the energy is then re-radiated in the form of thermal energy. The net balance between the former, the latter and the incident solar radiation determines the thermal evolution of the planetary subsurface (DePater 1990, 1991). However, the planetary thermal emissions do not strictly follow a blackbody curve due to the frequency dependence of the surface emissivity and the temperature gradients in the atmosphere or subsurface (Kellermann 1966). Venus has a thick atmosphere dominated by CO₂ ($\sim 96\%$). Due to the resulting Greenhouse effect, the surface temperature of Venus is ~ 735 K. The microwave/radio observations at cm/dcm wavelengths have the potential to probe deeper into the planetary

atmosphere and its surface. The thermal radiation from the planet has contributions from its atmosphere and the surface beneath it. The atmosphere is transparent enough at longer wavelengths that it permits the probing of planetary subsurface (Muhleman et al. 1973; Warnock & Dickel 1972; Butler et al. 2001). Also, at the long wavelengths, the surface reflectivity of the Venus is nearly a constant and is fairly low (~ 10 -15%) (Goldstein et al. 1965), markedly reducing the component of atmospheric emission reflected from the surface.

The presence of thick atmosphere and acid clouds prevent the surface probing apart from the IR windows between 0.9 to 2.5 μm (Allen & Crawford 1984; Meadows & Crisp 1996). Spectroscopic techniques have been used to study the Venusian upper atmosphere and its constituents as well as the presence of H₂SO₄ droplets of $\sim 1 \mu\text{m}$ size in the Venusian clouds (Hansen & Hovenier 1974; Kawabata & Hansen 1975). The VIRTIS probe onboard Venus Express mission had dedicated channels of 0.9, 1.1, 1.18 μm to study variations of the surface skin temperature of Venus (Drossart et al. 2004) and were used to identify hotspots on the surface of Venus, which form the direct evidence of recent volcanic activities (Smrekar et al. 2010).

Mayer et al. (1958) pioneered the microwave probing of the Venus disk at 3.15 cm wavelength and reported an unex-

* E-mail: c_sureshraj@vssc.gov.in

pectedly warm temperature of 560 ± 73 K, following this, several observations were carried out of the planet over a wide range of wavelengths in the mm, cm and meter regime. The initial observations of Venus were in visible spectra and had the popular assumption about the planet being similar to Earth. The mm/sub-mm wavelength observations are ideal for probing the planetary middle and upper troposphere (Devaraj & Steffes 2011). These have been used to study the Sulfur bearing molecules which affect the thermodynamics of the Venusian atmosphere (Butler et al. 2001). At shorter wavelength regime (mm-cm), the emission is largely dominated by the colder region of the Venus atmosphere (DePater 1991). At the longer cm-dcm wavelengths, the emission has the signature of the surface and subsurface thermophysical and electrical properties of the regolith. The values of the brightness temperature, T_b , increases from ~ 505 K at 1.3 cm to 680 K at 6.2 cm and then decreases at longer wavelengths (Butler et al. 2001). The recent radiometric observation at higher dcm/m wavelength observations using the GMRT reported T_b values of 526 ± 22 K, 409 ± 33 K, and < 426 K at 49 cm, 90 cm and 1.23 m, respectively, which indicate further decrease in the observed T_b (Mohan et al. 2017).

Neglecting atmospheric contributions, the radiometric observations of Venus measure its blackbody equivalent temperature or brightness temperature, which is a function of surface dielectric properties, temperature and roughness. While measurements of the total intensity (Stokes parameter, I) are related to the T_b of a planetary disk, the polarimetric observations are necessary to derive all the four Stokes parameters (I, Q, U, V) for studying surface properties like the dielectric permittivity and roughness. The emission from the surface of a planetary body is polarised due to the difference in the two orthogonal components of the electric field vector (perpendicular and parallel to the plane of incidence) at the air-surface interface (Troitskii 1954; Clark & Kuz'min 1965). The difference between these two orthogonal components at the larger angle of incidence is manifested as an enhancement in the degree of polarisation (DOP) towards the limb. Also, the emission becomes depolarised with increasing surface roughness (Pollack & Sagan 1965). Troitskii (1954); Davies & Gardner (1966) used the polarisation observations of the lunar surface to derive its dielectric constant (ϵ) and the surface roughness, which was followed by Heiles & Drake (1963) for deriving the surface dielectric constant of Venus. Several radio and radar observations were conducted to derive the dielectric properties of the Venus surface. Assuming the Venusian surface to be significantly smooth at cm/dcm wavelengths (Carpenter 1964), Clark & Kuz'min (1965) reported the ϵ of Venus ~ 2.5 at 10.6 cm wavelength. Later, Muhleman et al. (1979) estimated the ϵ as 4.1 based on: (i) value of the radio brightness of Venus measured with the Owens Valley interferometer, (ii) its radar reflectivity using the Arecibo radar and (iii) Mariner 5 and 10 occultation observations. Chapman (1986) measured the degree of polarisation across Venus from observations made at 21 cm using the Very Large Array (VLA) and obtained a value of 2.15. Pettengill et al. (1988) found that the lowland regions on Venus are characterized by $\epsilon = 5.0 \pm 0.9$ from the Pioneer-Venus radar altimetry experiment. Further, Pettengill et al. (1992) used the Magellan radiometer observations at 12.6 cm wavelength and determined the

global mean value of its emissivity as 0.845 that corresponds to a dielectric permittivity of between 4.0 and 4.5 depending on its surface roughness.

This paper describes the observations of Venus made close to its inferior conjunction in 2015 with the Giant Metrewave Radio Telescope (GMRT) with two objectives: (a) to determine values of its brightness temperature at 1297.67 MHz (~ 23 cm), 607.67 MHz (~ 49 cm) and ~ 233.67 MHz (~ 1.28 m) and (b) to estimate value of the dielectric constant of its surface from polarisation observations at 1297.67 MHz and 607.67 MHz. Section 2 describes the GMRT observations, followed by a description of the data reduction and analysis procedure in Section 3. The results are described in Section 4. Sections 5 and 6 present the discussion and conclusions, respectively.

2 OBSERVATION

Observations of Venus were carried out on four days, near its inferior conjunction in 2015, with the GMRT at frequencies centred at 233.67 MHz, 607.67 MHz and 1297.67 MHz (Table 1). The GMRT is an aperture synthesis radio telescope consisting of 30 fully steerable parabolic dish antennas, each with a diameter of 45 m. Fourteen dishes are located in a central array of ~ 1 km size and the other sixteen along three arms of a nearly Y-shaped array ~ 25 km in extent (Swarup et al. 1991). Dual orthogonal dipole feeds operating at 606, 325, 235 and 150 MHz measure linear polarisations which are converted to the left and right-handed circularly polarised signals using a quadrature hybrid. The horn type antennas operating in the 1000-1450 MHz frequency band directly measure orthogonal circular polarisations, and a quadrature hybrid is used to convert them to X and Y linear polarised signals. The GMRT correlator can provide all four cross-products for both linearly and circularly polarised signals and allows determination of all Stokes parameters, I, Q, U and V (Chengalur 2013).

Full polarimetric data was recorded for the two higher frequencies, and only total intensity (Stokes I) data was recorded for 233.67 MHz as the polarised emission at this frequency is insignificant compared to the noise contributed by the sky background and the electronics system. The observation procedure described by Mohan et al. (2017) was adopted for the current observations. Instead of tracking Venus, whose right ascension (RA) and declination (Dec) varied during the observations, the GMRT antennas tracked the mean position of its RA and Dec. For weak non-sidereal sources, this is the preferred strategy as it allows one to use the background celestial sources present in the field of view for self-calibration (Cornwell & Fomalont 1999). Self-calibration allows one to take into account the time-varying complex antenna gains (phase and amplitude), resulting from variations of the gains of the GMRT electronics and those due to the ionosphere, and leads to a much higher imaging dynamic range and fidelity. This is especially helpful at low radio frequencies, where the Galactic synchrotron background as well as the bulk of cosmic extragalactic source grow increasingly brighter due to their negative spectral index. The ephemeris details of Venus during the observations are given in Table 2. These observations were timed to be close to the inferior conjunction of Venus, when the

observed flux density of Venus would be the largest and so would be the apparent size of the disc of the planet. This led to an improved SNR and a larger number of synthesized beams across the planet, and thus enabled the most detailed and sensitive observations possible with the GMRT. Table 3 gives details of the calibrator sources used for the GMRT observations. The compact radio sources 0943-083, 1021+219, 0842+185 and 0842-185 were chosen for calibrating phases. For polarisation calibration, a single scan of 3C138 was observed near the middle of observations for ~ 10 min and also a single scan of 3C286 was made at the end of observations of Venus. Values of the fractional polarisation and polarisation angles for 3C138 and 3C286 used were given by Perley & Butler (2013) and are listed in Table 4.

3 DATA ANALYSES

Except for the polarisation calibration, the procedures involved and followed in the data analyses are detailed in Mohan et al. (2017). Brief discussions of these procedures are given in this Section for completeness. GMRT data were analysed using the Common Astronomical Software Application (CASA) package (McMullin et al. 2007). An integration time of 2 second was chosen to facilitate the removal of the fast varying radio frequency interference and then averaged to 16 seconds. A spectral resolution of 125 kHz was used for the observations. The polarisation observations at low frequencies are sensitive to variations of the ionospheric total electron content (TEC) over the GMRT line of sight, which can be determined from the GNSS and GPS measurements (<ftp://cddis.gsfc.nasa.gov/gnss/products/ionex/>). Using CASA recipes, the global TEC variation map over the GMRT sky for these observation days were generated and then applied to the measurement set using the task GENCAL. Perley & Butler (2013) flux density scale was applied for observations made at 607.67 MHz and 1297.67 MHz, whereas Scaife & Heald (2012) flux density scale was used for 233.67 MHz observations. The initial frequency and time-dependent complex gain solutions were obtained using the tasks BANDPASS and GAINCAL. Polarisation calibration was done prior to scaling the flux of the compact calibrator sources (task FLUXSCALE). Standard steps recommended for routine polarimetric continuum analysis were followed (e.g. as described in https://casaguides.nrao.edu/index.php/VLA_Continuum_Tutorial_3C391-CASA5.0.0 for the analysis of VLA P-band continuum data), and are briefly described below.

Polarisation calibration was performed for removing instrumental contribution to the observed polarisation. This involved solving for the unknown instrumental polarisation as well as calibrating the absolute polarisation position angle. After the task SETJY the model fluxes of the Stokes parameters Q and U of the polarisation calibrators were derived from the relation:

$$\begin{aligned} I_0 &= \text{Total Intensity} \\ Q_0 &= P_0 \cos(2\chi\pi/180) \\ U_0 &= P_0 \sin(2\chi\pi/180) \end{aligned}$$

where P_0 , the fractional polarisation and χ = polarisa-

tion position angle for 3C138 and 3C286 (Table 4). Using these parameters, the polarisation models were generated for 3C138 and 3C286. The cross-hand delay calibration using the strong unpolarised source 3C147, to account for the delay difference between the two orthogonal polarisations of the reference antenna was carried out. Any antenna has some polarisation leakage associated with it. This, along with the imperfections in the electronics chain, gives rise to a spurious polarisation, which makes even an unpolarised source appear somewhat polarised. This frequency dependent instrumental leakage term (D-term) was determined using the source 3C147. In order to obtain accurate polarisation position angle, the two orthogonal phases need to be calibrated. For this, the phase calibrator having significant parallactic angle coverage was utilized due to the fact that the point source is not 100% unpolarised. Afterwards, the flux of the phase calibrator sources was determined using the task FLUXSCALE. The parallactic angle corrections for all the data were done while applying the calibration solutions to the measurement set, using the PARANG parameter in APPLYCAL.

Imaging: The background celestial radio sources in the field of view of the GMRT antennas were used for the self-calibration as described by Mohan et al. (2017) in the imaging procedure Section. The procedure was continued until the gain phases varied within ± 5 degrees. Next, the CLEAN components were subtracted from the maps using the task UVSUB. One-minute snapshots of Venus in all the four Stokes parameters were generated after compensating for the non-sidereal motion of Venus. The co-added maps of Venus were then deconvolved using the point spread function corresponding to the entire observation, followed by a convolution using the corresponding restoring beam. The uncertainty in the estimated flux density is contributed by - pointing errors, temporal variation of the gain of the system and the errors due to uncertainties in flux values of the calibrators due to flux density scale used. The detailed error estimation is presented in Mohan et al. (2017). All of the above factors together can lead to systematic error of about 7% in the measured flux density of Venus.

Besides the above corrections, the Galactic background temperature (T_{gal}), corresponding to the location of Venus on the day of the observation was estimated from the 408 MHz map by Haslam et al. (1981). A spectral index of -2.6 ± 0.15 (Reich & Reich 1988) was used to scale the T_{gal} values corresponding to the GMRT frequencies. The values of T_{gal} were determined as 6 ± 1 K, 5 ± 1 K, and 64 ± 8 K for July 25 (607.67 MHz), August 29 (607.67 MHz) and July 26 (233.67 MHz) observations, respectively. For the 607.67 MHz and 1297.67 MHz observations, the background temperature is a sum of the galactic background and cosmic microwave background temperature, which are $\sim 6 + 2.7 \sim 9$ K, $\sim 5 + 2.7 \sim 8$ K, $\sim 1 + 2.7 \sim 4$ K for July 25 (607.67 MHz), August 29 (607.67 MHz) and September 06 (1297.67 MHz), respectively, are also accounted for.

The consistency of the images was then evaluated by grouping the 1-minute snapshots into two time bins and independently coadding. It was found that, for 25th July and 29th August (607.67 MHz) the observed the flux density was consistent within 2% while for 1297.67 MHz and 233.67 MHz the flux densities were consistent within a factor of $\sim 3\%$ and $\sim 5\%$, respectively.

Table 1. GMRT campaign for observations of Venus 2015

Central Frequency (MHz)	Date	Bandwidth (MHz)	No. of working antennas	Observing time on Venus (mins)	Stokes
607.67	July 25	33.33	28	5.5	I, Q, U, V
233.67	July 26	16.67	27	6.5	I
607.67	August 29	33.33	28	6.0	I, Q, U, V
1297.67	September 06	33.33	28	6.5	I, Q, U, V

Table 2. Ephemeris data for GMRT campaign for observations of Venus 2015

Central Frequency (MHz)	Date	Venus Angular Diameter (θ) (arcsec)	Right Ascension (mid-observation) (h:min:s)	Declination (mid-observation) (deg.arcmin.arcsec)	Sub Earth Latitude	Sub Earth Longitude (deg East)	Phase
607.67	July 25	47.43	10:05:12	+07.47.39	4.34	307.6	0.13
233.67	July 26	48.16	10:04:49	+07.35.31	4.56	309.06	0.12
607.67	August 29	53.33	09:02:25	+08.37.39	8.23	344.16	0.068
1297.67	September 06	48.02	08:58:21	+09.51.16	7.31	354.65	0.14

Table 3. Details of calibrators for GMRT campaign for observation of Venus 2015

Date	Frequency (MHz)	Flux calibrator	polarization calibrator	Phase calibrator
July 25	607.67	3C147, 3C286	3C286, 3C138	0943-083
July 26	233.67	3C147, 3C286		1021+219
August 29	607.67	3C147, 3C286	3C286, 3C138	0842+185
September 06	1297.67	3C147, 3C286	3C286, 3C138	0842+185

4 RESULTS

4.1 Brightness temperature of Venus

The GMRT observations of Venus were made in 2015, with primary objective of observing the planetary thermal emission for a longer period during the inferior conjunction of Venus, when it is closest to Earth. During this observation period, the planet had an angular diameter of $\sim 50''$ which is almost twice that during the 2004 observations, and the observation duration was also almost double that of the 2004 observations. All these factors have significantly improved signal to noise ratio while extending the GMRT observation towards a higher frequency, at 1297.67 MHz. Table-5 presents the results of the flux density and T_b measurements of the Venus. Columns 3 and 4 give the size and the position angle of the synthesized beam respectively. Column 5 gives the observed background *rms* values in the map of Venus. There is an improvement of ~ 5 times in the signal to noise ratio in the maps derived at 607.67 MHz from the 2015 observations, compared to that from the 2004 observations, owing to the closer proximity of the planet. Columns 6 and 7 give the measured flux density of Venus and the estimated error of its flux density. Column 8 gives values of T_b , that were derived using the Rayleigh-Jeans relation, measured flux density and solid angle subtended by Venus. Estimated values of T_{gal} are given in Column 9. Column 10 gives the corrected values of Venus T_b by adding T_{gal}

values and microwave background temperature value for the 233.67 MHz, 607.67 MHz and 1297.67 MHz observations. In Column 11 are given estimated values of the T_b in bold and also their estimated errors as derived by adding the quadrature sum of the random errors as determined from column 7 and the systematic error of 7%.

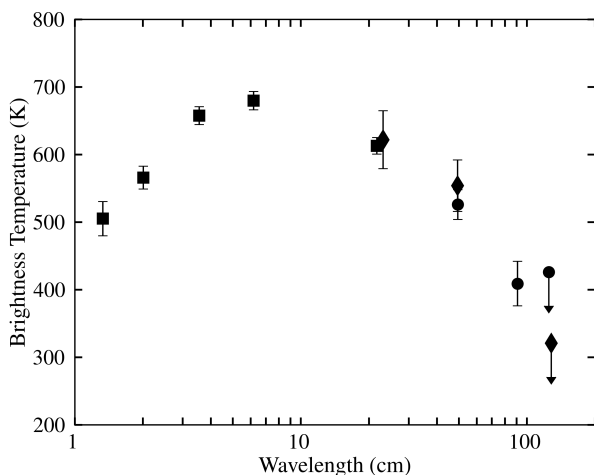
The total intensity maps of the Venus were generated for the respective days of observations. The observed T_b variation ranges from ~ 100 K near the limb, peaking at ~ 650 K around the centre of the disk for the 25 July and ~ 100 K to ~ 700 K for the 29 August 607.67 MHz observations. In case of 1297.67 MHz, the T_b ranges from ~ 200 K near the limb to >750 K near the centre of the disk, indicating a brighter Venus at 1297.67 MHz frequency. As described in Table 5, the mean values of T_b are found as 554 ± 38 K at 607.67 MHz and 622 ± 43 K at 1297.67 MHz, respectively.

In the case of the 233.67 MHz observations made on 26 July 2015, a strong 3C source of ~ 10 Jy was present near the half maximum position of the GMRT primary beam limiting the dynamic range of the deconvolved image, whence Venus was buried in the map noise. Hence, an upper limit of 3σ was chosen for the expected flux density of Venus at 233.67 MHz as shown in row 3, column 6 in Table 5.

The T_b values of Venus obtained from the 2015 observations are plotted in Fig. 1 along with the T_b observations made with the VLA by Butler et al. (2001) and those using the GMRT by Mohan et al. (2017). These observations

Table 4. Details of polarization properties of Calibrator sources for observation of Venus 2015

Freq (MHz)	3C138 % Pol	Pol ang	3C286 % pol	Pol ang
607.67	3.9	-26	7.6	33
1050.0	5.6	-14	8.6	33
1297.67	6.7	-12	9.1	33
1450.0	7.5	-11	9.5	33

**Figure 1.** Summary of T_b measurements on Venus in cm-dcm wavelengths. The solid square (■) represents the observation by Butler et al. (2001) using the VLA. The solid circles (●) represent the observation by Mohan et al. (2017) using the GMRT and the current observations are illustrated by the solid diamond (◆) points.

show that T_b peaks at ~ 680 K at a wavelength of 6 cm and then decreases steadily to 622 K at 23 cm, 554 K at 49 cm, 409 K at 91 cm and to < 321 K at 128 cm. The T_b values obtained by GMRT at 1297.67 MHz are consistent with the VLA observations made by Butler et al. (2001). Also, the T_b at 607.67 MHz agrees well with that reported by Mohan et al. (2017) based on GMRT observations in 2004. The result obtained from the current observations at 233.67 MHz establish that the T_b continues to decrease even at wavelengths beyond one metre.

4.2 Degree of polarization measurement of Venus

The degree of linear polarisation (or fractional polarisation) of any planetary surface medium represents the fraction of the linearly polarised component of the total intensity of radiation. The properties of thermal radiation (including polarisation) are dependent on the surface roughness, surface dielectric permittivity and its discontinuity in the horizontal and vertical directions within the penetration depth of the wave. Therefore, the degree of polarisation (DOP) measurements are carried out to study the dielectric properties and surface roughness parameters. The fraction of DOP can be

obtained from the observations of Stokes I, Q, and U parameters as:

$$m = \frac{\sqrt{Q^2 + U^2}}{I} \quad (1)$$

where the numerator corresponding to the linear polarization intensity ($P = \sqrt{Q^2 + U^2}$) is the total intensity of the linear polarized component of the radiation. The Stokes parameters measured at 607.67 MHz and 1297.67 MHz are used to derive the DOP of Venus during the computation.

Figures 2 and 3 show the variations of the DOP across the disk of Venus from the observations made at 607.67 MHz on 25 July 2015 and at 1297.67 MHz on 06 September 2015. Division of the polarisation intensity by Stokes parameter I lead to exceptionally high values of the DOP outside the disk of Venus and has no physical significance. This was countered by masking the degree of polarisation outside the disk by setting a threshold of 3σ in the total intensity maps, where σ is the *rms* of intensity map. The DOP increases steadily from the centre of the disk towards its limb. At 607.67 MHz the mean value of DOP increased from $\sim 5\%$ to $\sim 22\%$, and that at 1297.67 MHz from $\sim 5\%$ at the centre to $\sim 32\%$ towards the limb (refer Section 4.3). The DOP variations, with the contour lines overlaid to quantify the DOP are shown in these figures. Under the assumptions of a smooth planetary surface with respect to the probing wavelength and the magnetic permeability $\mu = \text{unity}$, the dielectric permittivity, ϵ , of the Venus surface can be estimated from the measured DOP values and is described in the next Section.

4.3 Estimation of the dielectric constant of Venus surface

For reflection/refraction from a plane dielectric interface, the theoretical values of the DOP are related to perpendicular and parallel components of the surface reflectivity (Davies & Gardner 1966; Born & Wolf 1980):

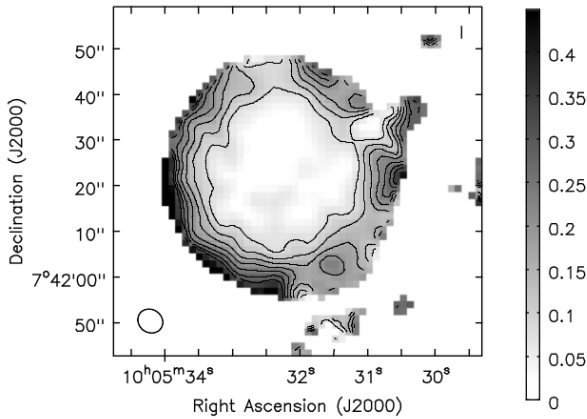
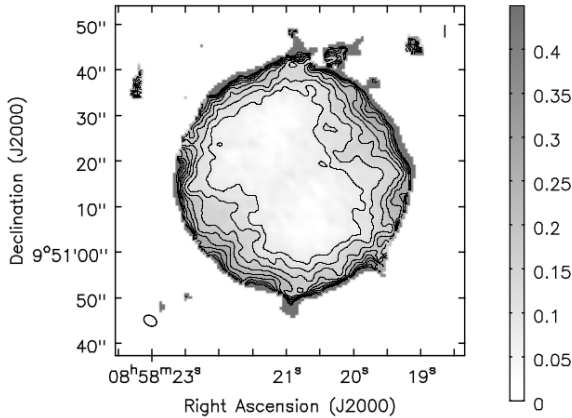
$$m = \frac{\frac{1}{2}(R_{\perp} - R_{\parallel})}{1 - \frac{1}{2}(R_{\perp} + R_{\parallel})} \quad (2)$$

where R_{\perp} and R_{\parallel} are, respectively, the perpendicular and parallel component of power reflection coefficients or the reflectivity of the electromagnetic radiation at the plane of incidence and are given by the square of the Fresnel's equation.

$$R_{\perp} = \left| \frac{\cos\theta_i - \sqrt{(\epsilon - \sin^2\theta_i)}}{\cos\theta_i + \sqrt{(\epsilon - \sin^2\theta_i)}} \right|^2 \quad (3)$$

Table 5. Summary of T_b measurements (2015)

Frequency (MHz)	Date (2015)	Beam Size (arcsec)	Beam Position Angle (degree)	Map rms (mJy)	Flux (mJy)	Δ Flux (mJy)	T_b (K)	T_{gal} (K)	$T_{b,cor}$ (K)	mean $T_{b,cor}$ (K)
233.67	Jul 26	$12.66'' \times 10.8''$	55.1	1.52	18.18	6.27	$\downarrow 249$	64 ± 8	$\downarrow 321$	$\downarrow 321$
607.67	Jul 25	$5.67'' \times 5.03''$	62.6	0.16	251.087	0.75	533.06	6 ± 1	543	554 ± 38
607.67	Aug 29	$6.14'' \times 4.28''$	46.8	0.21	330.36	1.10	557.23	5 ± 1	566	
1297.67	Sep 06	$2.98'' \times 2.22''$	61.9	0.22	1354.00	2.05	618.13	4	622	622 ± 43

**Figure 2.** Contour plot of degree of polarization across Venus at 607.67 MHz made on 25 July 2015. Contour Values: 8, 12, 16, 20, 24 and 28 percent**Figure 3.** Contour plot of degree of polarization across Venus at 1297.67 MHz on 06 September 2015. Contour values are 8, 12, 16, 20, 24, 28, 32, 36 and 40 percent

$$R_{||} = \left| \frac{\varepsilon \cos \theta_i - \sqrt{(\varepsilon - \sin^2 \theta_i)}}{\varepsilon \cos \theta_i + \sqrt{(\varepsilon - \sin^2 \theta_i)}} \right|^2 \quad (4)$$

where the angle of incidence $\theta_i = \sin^{-1}(r/R_{\text{disk}})$, where ‘ r ’ is the radial distance from the centre in arcsec and R_{disk} is the angular radius of the disk of Venus in arcsec.

The pixel sizes of the images were chosen as 0.6 arcsec

and 1.5 arcsec, respectively, for the 1297.67 and 607.67 MHz observations. In the observed DOP maps shown in Figs. 2 and 3, we first selected concentric annular regions, each of width of 1 arcsec at 1297.67 MHz and 2 arcsec at 607.67 MHz observations, starting from the centre all the way to the limb of Venus. The angle of incidence corresponding to the mean radii of these concentric annular sections varied from 0 to a maximum of ~ 67 degrees from the centre towards the limb at 607.67 MHz and that from 0 to a maximum of ~ 74 degrees at 1297.67 MHz. The mean and the standard deviations of the DOP for each of the annular sections were then determined.

It is assumed that each pixel in the annular sections is statistically independent. However, since the FWHM of the GMRT beam = ~ 6 arcsec for 607.67 MHz and ~ 3 arcsec for 1297.67 MHz, the beam can occupy ~ 20 pixels and ~ 12 pixels for 1297.67 and 607.67 MHz, respectively, on the Venusian disk. But, due to the overlap of the beams on the adjacent annulus the number of independent pixels of DOP occupying the beam were determined to be approximately $1/3^{\text{rd}}$ and $1/4^{\text{th}}$ of the total number pixels in each annular region, respectively, at 1297.67 and 607.67 MHz. Later, the standard deviation was divided by the revised value of the number of independent pixels, N and the standard error was found out as Standard Deviation/ \sqrt{N} . The variation of the DOP with increasing radial distance from the centre of Venus disk was examined by plotting the mean value of DOP in each annular region. In Figs. 4 and 5, using filled circles, are shown the mean values of the DOP and the vertical bars are the standard error derived as a function of the radial distance from the centre for observations made at 607.67 MHz on July 25 and at 1297.67 MHz on September 6, respectively. The key point is that the error bars reflect only the random component of the uncertainties in the Figs. 4 and 5, while the departure of the degree of polarisation from zero close to the centre of the disk arises because of systematics.

These figures also include the theoretical values of the DOP that were derived by using the Equations 3, 4 and 5 and then convolved with a Gaussian having FWHM corresponding to the synthesized beam of GMRT. These are shown by solid lines for four different values of the ε ranging from 3.5 to 5.5, with increments of 0.5. The statistical technique of Chi-square minimization is used to identify the ε corresponding to the best fit from the various values ranging from 2.5 to 6.0 and the value of ε corresponding to the best fit was obtained as 4.5 at 607.67 as well at 1297.67 MHz.

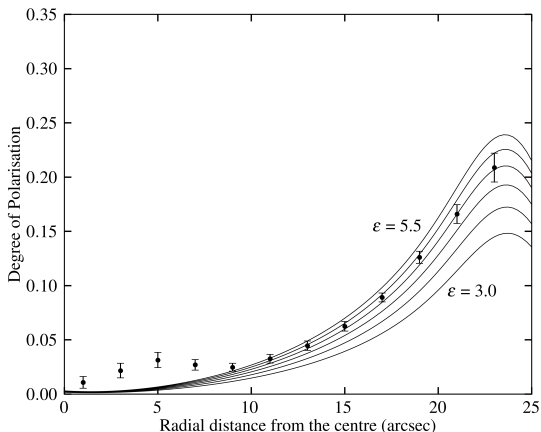


Figure 4. Variation of the observed degree of polarization with respect to the radial distance from the centre at 607.67 MHz as observed on 25 July 2015 (solid dots). Solid lines show the theoretical curves convolved with Gaussian corresponding to the GMRT synthesized beam plotted for $\epsilon = 3.0, 3.5, 4.0, 4.5, 5.0$ and 5.5

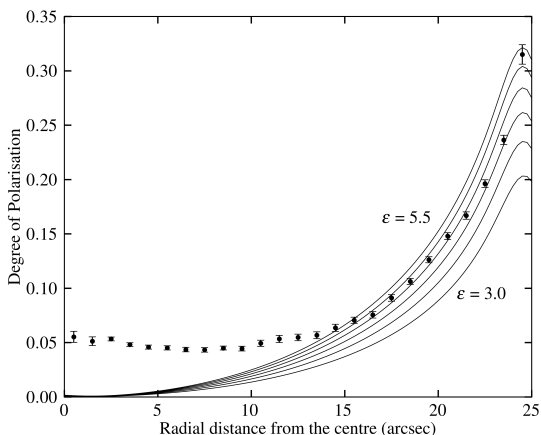


Figure 5. Variation of the observed degree of polarization with respect to the radial distance from the centre at 1297.67 MHz as observed on 06 September 2015 (solid dots). Solid lines show the theoretical curves convolved with Gaussians corresponding to the GMRT synthesized beam plotted for $\epsilon = 3.0, 3.5, 4.0, 4.5, 5.0$ and 5.5

5 DISCUSSIONS

In Figure 1 are given observed values of the T_b of Venus measured with the VLA by Butler et al. (2001) and that from the GMRT observations. Combining the results of these two radio interferometers provide observations of Venus over a wide range of wavelength, from 1.3 cm to 128 cm. The timing of the presented 10 hour GMRT observations was optimised to be close to the inferior conjunction of the planet, which enabled an improvement in SNR by factor of five and an increase in the number of resolution elements across the disc of the planet by a factor >4 , when compared to the previous observations. The T_b of <321 K obtained in the current GMRT

campaign at 128 cm is considerably lower than that reported by Mohan et al. (2017), and that at 23 cm is consistent with the earlier measurements by Butler et al. (2001). These analyses indicate that the thermal emission from the Venus surface and subsurface continues to decrease in the dcm and m wavelength domain of the electromagnetic spectrum. Several attempts have been made to explain the observed decreasing trend of the T_b of Venus (Barrett & Staelin 1964; Muhleman et al. 1979). Butler et al. (2001) considered atmospheric opacity as well the surface temperature of Venus for explaining observed values of T_b at cm wavelengths and got good agreement till the wavelength upto ~ 6 cm. However, they were not able to explain the observations at dcm and m wavelengths. Warnock & Dickel (1972) proposed a two-layer model, i.e. a layer of soil overlaying a regolith having a different dielectric values. They also noted that the observed decrease of T_b at these wavelengths is unlikely to arise from a lower value of the physical temperature of the subsurface in view of thick overlying hot atmosphere. The constant surface temperature of ~ 735 K resulting from the Greenhouse effect is quite likely to heat the sub-surface of Venus over the millions of years. A radiative transfer (RT) analysis may be fruitful for explaining the observed decreasing values of T_b at decimetre and metre wavelengths, considering the likely variation in the dielectric properties of the Venusian subsurface.

The mean value of DOP derived near the limb of Venus at 1297.67 MHz (Fig. 3) is about 32% compared to the value of $\sim 22\%$ at 607.67 MHz (Fig. 2) owing to a higher angle of incidence due to the better angular resolution at 1298.76 MHz. A DOP of 3-5% is observed close to the centre of the disk. Ideally, the DOP near the centre of the map is expected to be zero due to the rotational symmetry of the polarised radiation. However, the intensity of polarised emission, is given by $P = \sqrt{Q^2 + U^2}$. This quantity can never be negative and hence there is a non-zero mean positive bias to the noise (Chapman 1986). The noise on the polarised intensity near the centre is of the order of the background noise which is prevalent throughout the map. This noise is ~ 0.1 mJy for 607.67 MHz and ~ 0.15 mJy for 1297.67 MHz and leads to the observed small values of DOP close to the centre of the disc. In Figs. 4 and 5, the observed DOP begins to match with the theoretical values beyond ~ 10 arcsec for July 25, 607.67 MHz and for September 06 at 1297.67 MHz observations when the signal begins to dominate the noise.

The value of the Venus surface dielectric constant is estimated from the DOP maps of Venus generated from the GMRT dataset and the theoretical calculations to be, ~ 4.5 both at 1297.67 MHz and 607.67 MHz. These are lowest frequency polarimetric observations of Venus, and can hence probe the subsurface deeper than has been possible before. Earlier estimates of dielectric constant have yielded varied from 2.5 to 5.0 (Clark & Kuz'min 1965; Muhleman et al. 1979; Pettengill et al. 1988). Our observations are consistent with the radar observations of Venus by several workers including the Magellan observations determined the values of the dielectric constant to lie between 4 and 4.5 for the surface of Venus (Pettengill et al. 1992). The dielectric constant derived from the DOP observations depends on: 1) the relative surface roughness with respect to the probing frequencies (Golden 1979) and 2) dielectric constant variation within the penetration depth due to the increase in the bulk

density (Ulaby et al. 1990). The effect of frequency on dielectric constant was ruled out by Campbell & Ulrichs (1969), based on their measurements of the dielectric constant of planetary rocks including the basalt type over a wide range of frequency from 450 MHz to 35 GHz. Owing to the deeper penetration depth (nearly ten times the wavelength) in a planetary dry surface at dcm and m wavelengths, a variation of the regolith bulk density of Venus is a valid possibility. As the real part of dielectric constant of the dry planetary regolith are related to only the bulk density, it can vary from ~ 2.0 to ~ 8.0 (Ulaby et al. 1990) with the variation of bulk density from very loose (regolith) condition to highly packed condition close to rock material. Due to the presence of greenhouse gases for millions of years, any drastic variation in the temperature of Venus subsurface regolith up to tens of metres is very unlikely. Also at these wavelengths, the surface could be relatively smoother and the effect of surface roughness can be neglected, leading to the estimated value of dielectric very close to the real value. As the dielectric constant plays a major role in the observed T_b at various frequencies, the current results form an essential input for the radiative transfer based models for exploring the role of subsurface properties (temperature and dielectric properties through density and mineral content) on thermal emissions and the decrease in T_b with wavelength at cm/dcm wavelengths.

6 CONCLUSION

From the observations of thermal emission from Venus surface made with the GMRT at 1297.67 MHz (23 cm), 607.67 MHz (49 cm) and 233.67 MHz (1.28 m), the disc averaged brightness temperature, T_b , values were derived as 622 ± 43 K, 554 ± 38 K and upper limit of 321 K, respectively at the above frequencies. Considering also measurements made by previous workers using the VLA, it is found that T_b is ~ 505 K at 1.3 cm, peaks at ~ 680 K at a wavelength of 6 cm and then decreases continuously with increasing wavelengths to < 321 K at 1.28 m. A satisfactory model to explain the observations should consider the likely penetration depth of radiation at decimeter and centimeter wavelengths in the dielectric medium of Venus. We also present the polarimetric observations of Venus at the lowest frequency set, which allows us to probe deeper into the subsurface. Using Stokes parameters derived from these observations, the DOP maps of Venus were generated at 1297.67 MHz and 607.67 MHz. A combined analysis of observed DOP and theoretically derived DOP, the dielectric constant of the surface of Venus was found to be ~ 4.5 at both 1297.67 MHz and 607.67 MHz. This is consistent with those derived from the orbiter-based radar observations of Venus which lie in the range 4 - 4.5 for the surface of Venus.

ACKNOWLEDGEMENTS

Authors thank the Reviewer Dr Peter G. Ford, Assistant Editor and Scientific Editor for several valuable suggestions for improvements on this paper. Authors thank Dr. Subhasish Roy and Dr. Niruj Mohan Ramanujam of NCRA and Dr. Nizy Mathew of SPL, VSSC for their valuable comments and

wholehearted support throughout the work. Authors thank the staff of the GMRT who made these observations possible. The GMRT is run by the National Centre for Radio Astrophysics of the Tata Institute of Fundamental Research. Mr. Nithin Mohan is supported by an ISRO Research Fellowship.

REFERENCES

- Allen D., Crawford J., 1984, *Nature*, 307, 222
 Barrett A., Staelin A., 1964, *Space Science Reviews*, 3, 109
 Born M., Wolf E., 1980, *Principles of Optics: Electromagnetic Theory of Propagation, Interference and Diffraction of Light*, 6 edn. Pergamon
 Butler B., Steffes P., Suleiman S., Kolodner M., Jenkins J., 2001, *Icarus*, 154, 226
 Campbell M., Ulrichs J., 1969, *J. Geophys. Res.*, 74
 Carpenter R., 1964, *AJ*, 69, 2
 Chapman B., 1986, PhD thesis, Massachusetts Institute of Technology, <http://hdl.handle.net/1721.1/14886>
 Chengalur J., 2013, Technical report, NCRA Technical Report, NCRA/COM/OD. Technical Report. National Centre for Radio Astrophysics, Pune 411007, India
 Clark B., Kuz'min A., 1965, *ApJ*, 142, 23
 Cornwell T., Fomalont E., 1999, *Synthesis Imaging in Radio Astronomy*, II edn. ASP Conference Series, pp 187–199
 Davies R., Gardner F., 1966, *Aust. J. Phys.*, pp 823–836
 DePater I., 1990, *ARA&A*, 28, 347
 DePater I., 1991, *Physics Reports*, 200, 1
 Devaraj K., Steffes P., 2011, *Radio Science*, 46
 Drossart P., et al., 2004, *Infrared Space-borne Remote Sensing XII*
 Golden L., 1979, *Icarus*, 38, 451
 Goldstein R., Stevens R., Victor W. K., 1965, Technical report, Radar Exploration of Venus: Goldstone Observatory Report Oct.-Dec. 1962. Goldstone Observatory
 Hansen J., Hovenier J., 1974, *Journal of the Atmospheric Sciences*, 31, 1137
 Haslam C., Salter C., Stoffel H., Wilson W., 1981, *A&A Supplement Series*, 47
 Heiles C., Drake F., 1963, *Icarus*, 2, 281
 Kawabata K., Hansen J., 1975, *Journal of the Atmospheric Sciences*, 32, 1133
 Kellermann K., 1966, *Icarus*, 5, 478
 Mayer C., McCullough T., Sloanaker R., 1958, *Proceedings of the IRE*, p. 260
 McMullin J. P., Waters B., Schiebel D., Young W., Golap K., 2007, in Shaw R., Hill F., Bell D., eds, *Astronomical Society of the Pacific Conference Series Vol. 376, Astronomical Data Analysis Software and Systems XVI*. p. 127
 Meadows V., Crisp D., 1996, *Journal of Geophysical Research*, 101, 4595
 Mohan N., Roy S., Swarup G., Oberoi D., Niruj M., Sureshraj C., Bhardwaj A., 2017, *Icarus*, 297, 119
 Muhleman D., Berge G., Orton G., 1973, *ApJ*, 183, 1081
 Muhleman D., Orton G., Berge G., 1979, *apj*, 234, 733
 Perley R., Butler B., 2013, *ApJ Supplement Series*, 206, 16
 Pettengill G., Ford P., Chapman B., 1988, *J. Geophys. Res.: Solid Earth*, 93, 14881
 Pettengill G., Ford P., R.J. W., 1992, *J. Geophys. Res.: Planets*, 97, 13091
 Pollack J., Sagan C., 1965, *ApJ*, 141, 1161
 Reich P., Reich W., 1988, *aap*, 196, 211
 Scaife A. M. M., Heald G. H., 2012, *MNRAS*, 423, 30
 Smrekar S., Stofan E., Mueller N., Treiman A., Linda E.-T., Helbert J., Piccioni G., Drossart P., 2010, *Science*, 328, 605

- Swarup G., Ananthkrishnan S., Kapahi V. K., Rao A. P., Subrahmanya C. R., Kulkarni V. K., 1991, *Current Science*, 60, 90
- Troitskii V., 1954, *Astr. Zh.*, 31
- Ulaby F. T., Dobson M. C., East J. R., Bengal T. H., Garvin J. B., Evans D. L., 1990, [IEEE Transactions on Geoscience and Remote Sensing](#), 28, 325
- Warnock W., Dickel J., 1972, [Icarus](#), 17, 682